Naval Research Laboratory
Washington, DC 20375-5320

NRL/MR/6790--99-8317

Feasibility Experiments for Underwater Shock and Bubble Generation with a High-Power Laser

THEODORE G. JONES

ICARUS Research, Inc.
Bethesda, MD

JACOB GRUN
H. RAY BURRIS

Beam Physics Branch
Plasma Physics Division

CHARLES MANKA

Research Support Instruaments, Inc.
Lanham, MD

April 22, 1999

REPORT DOCUMENTATION PAGE

Form Approved
OMB No. 0704-0188

1. AGENCY USE ONLY (*Leave Blank*)	2. REPORT DATE	3. REPORT TYPE AND DATES COVERED
	April 22, 1999	Interim Report

4. TITLE AND SUBTITLE

Feasibility Experiments for Underwater Shock and Bubble Generation with a High-Power Laser

5. FUNDING NUMBERS

JON - 67-6095-09

6. AUTHOR(S)

Theodore G. Jones,* Jacob Grun, Charles Manka,† and H. Ray Burris

7. PERFORMING ORGANIZATION NAME(S) AND ADDRESS(ES)

Naval Research Laboratory
Washington, DC 20375-5320

8. PERFORMING ORGANIZATION REPORT NUMBER

NRL/MR/6790--99-8317

9. SPONSORING/MONITORING AGENCY NAME(S) AND ADDRESS(ES)

Office of Naval Research
Arlington, VA 22217

10. SPONSORING/MONITORING AGENCY REPORT NUMBER

11. SUPPLEMENTARY NOTES

*ICARUS Research, Inc., P.O. Box 30780, Bethesda, MD 20824-0780
†Research Support Instruments, Inc., 4324B Forbes Boulevard, Lanham, MD 20706

12a. DISTRIBUTION/AVAILABILITY STATEMENT

Approved for public release; distribution unlimited.

12b. DISTRIBUTION CODE

A

13. ABSTRACT (*Maximum 200 words*)

High energy laser pulses (up to 150 joules at 527 nm) were directed onto underwater targets to produce a heated volume which, upon expansion, created underwater shocks and bubbles. These experiments were a feasibility study for a laboratory experimental program studying two phenomena: (1) bubble collapse dynamics in close proximity to a solid interface, and (2) shock propagation dynamics in aerated sand/water mixtures. The laser was focused both onto a point in the water and onto the surface of a solid thin foil target immersed in the water. For both types of targets, the focal volume of the laser beam was in water. Solid laser targets were observed to effectively localize laser energy deposition, providing a point shock source and producing spherical shocks. Shock pressures were inferred from shock propagation speeds to be 30 Kbar at 2 mm, and measured by carbon piezoresistive gauges to be 200 bar at 13 mm. Bubbles were formed with maximum radii of 15 mm and oscillation times of 3 ms. Key features of a design for a permanent experimental chamber are given in the report.

14. SUBJECT TERMS	15. NUMBER OF PAGES
Underwater laser shock	25
	16. PRICE CODE

17. SECURITY CLASSIFICATION OF REPORT	18. SECURITY CLASSIFICATION OF THIS PAGE	19. SECURITY CLASSIFICATION OF ABSTRACT	20. LIMITATION OF ABSTRACT
UNCLASSIFIED	UNCLASSIFIED	UNCLASSIFIED	UL

NSN 7540-01-280-5500

Standard Form 298 (Rev. 2-89)
Prescribed by ANSI Std 239-18
298-102

CONTENTS

Feasibility Experiments for Underwater Shock and Bubble Generation with a High-power Laser

Objectives

There were two main goals of FY98 work: 1) to demonstrate the feasibility of laser shock generation in water with a high power laser, and 2) the design of a permanent experimental chamber. In detail:

1) High Power Laser Shock Feasibility Experiment

Build an inexpensive temporary water-chamber. Verify shock launching in water with a 100-200 joule laser beam. (These energies are 2 orders of magnitude greater than laser energies used in previous published experiments to launch shocks in water.) Set up ruby pressure gauges or other pressure gauge diagnostics and characterize the shock strength as a function of distance from the explosion. Verify the sphericity of the shock. Demonstrate acceptable shot-to-shot reproducibility. Based on the shock strength, shape, and sphericity determine the spatial scale of subsequent experiments. Determine whether experiments can be performed by focusing though the side of the chamber only or whether provisions for focusing through the top or bottom must be built in.

2) Permanent Experimental Chamber Design and Construction

Design a permanent water chamber capable of containing and diagnosing the three experiments detailed in the FY97 Proposal: a) the shallow water mine problem; b) the bubble-planar surface interaction problem; and c) the double-hull problem. In particular, make sure the chamber accommodates the bubble experiment and the shallow water mine experiment. Evaluate the need for pressurizing the chamber or pulling a partial vacuum (for varying and scaling the effective depth) and implement as necessary. Incorporate into the design whatever lessons are learned in 1 above.

Manuscript approved March 30, 1999.

Results and Progress

1) High Power Laser Shock Feasibility Experiments

Experimental setup

Experiments to determine the feasibility and optimum configuration for laser shock initiation were performed in a small (approximately 80 liters in volume) temporary water tank. One beam of the Pharos laser was frequency-doubled to 527 nm, providing up to 150 J of energy in 5 ns. Shocks were produced at the beam focus, which was placed on two types of targets: 1) in the center of the water volume, and 2) on a solid target immersed in the water. The focal spot was less than 500 μm in diameter for both types of targets. Figure 1 shows a schematic of the experimental setup for laser shock generation, including the shock imaging diagnostic.

Water absorbs strongly at the 1.054 μm fundamental frequency of Pharos, with an attenuation length of 3 cm. Therefore, laser shock initiation with the Pharos laser was done with frequency-doubled light at 527 nm, which has an attenuation length of 50 m. Frequency doubling was done with a set of KD*P type II doubling crystals, providing efficiencies up to approximately 35% and yielding up to 150 J per beam at 527 nm[1].

Successful spherical shock and bubble formation depends on localizing laser energy deposition in a controlled and reproducible manner. This depends on being able to bring the laser beam to a reproducible focus with low absorption or scattering. A principal goal of these experiments was the determination of the optimal focusing geometry and medium to achieve this. At high laser intensities in high-density media such as water, beam instabilities or optical breakdown can cause absorption or diversion of the beam before it reaches focus. Therefore, the first question to be answered by these experiments is whether the laser beam can be focused in water or must be focused exclusively in vacuum.

---

[1] M. Pronko, et al., IEEE J. Quantum Electr. **26** (1990) 337.

Experience from previous high energy laser shock generation experiments in solids indicates that a vacuum focus is the most efficient configuration for laser shock coupling. A conical evacuated focusing chamber with a foil target will therefore be incorporated into the permanent experimental chamber. This focusing chamber will allow for beam entrance from the top of the chamber.

Some experiments such as those studying bubble collapse dynamics may require a minimal amount of solid structure near the laser focus. For these experiments a laser focus in water may be optimal. In this case, the beam path through the water (or any high density media), should be minimized to reduce the chance of incurring beam instabilities. This concern is especially relevant to the focusing volume where laser intensities are higher and the risk of beam instabilities is increased. Since the Pharos beam size and lens aperture are fixed, a short focal length and therefore small *f/#* were chosen (*f/#* = 1.2 in air, *f/#* = 1.6 in water) to minimize the water volume with high laser intensity. Since our laser energies and intensities are two orders of magnitude greater than any used previously for water shock hydrodynamics studies, diagnostic efforts in initial experiments were concentrated on the beam focusing volume.

Both the focusing lens and the chamber window should be anti-reflection (AR) coated for maximum laser energy transmission to the target. AR coatings are not designed for underwater use so that the best placement for the lens is in air, or possibly used as a window with only the air side AR coated. If a separate lens and window are used, the lens should be placed as close as possible to the window to minimize the beam intensity through the glass.

Initial laser shock initiation experiments used a single beam of Pharos. However, with two more Pharos beams available and one more KD*P doubling crystal available, there is a capability for using two Pharos beams in the final experimental configuration. Optimization of the KD*P crystal alignment has yielded efficiencies up to 55% in past experiments, providing a capability to increase laser energy up to approximately 250 J at 527 nm for one Pharos beam. The total energy on target can be 500 J with two beams.

Diagnostic Testing and Development

Shock Experiments in Solids

Fiber-optic ruby and carbon piezoresistive gauges were tested this fiscal year. These tests were especially important for the ruby gauges since these have never before been fielded to measure such short duration shock impulses ($\Delta t \leq 100$ ns at $r = 2$ mm). The ruby gauges are being implemented by NRL Code 6110. These gauges are fiber-optically coupled to a pump laser. The pressure-dependent spectral shift of a laser-induced fluorescence line is then tracked in time with a spectrometer and a streak camera. These gauges measure pressures from 1 to 200 kilobar. Plans for testing these gauges in water are included in the next experimental run.

To determine their time response, sensitivity, durability, and vulnerability to stray light, pressure gauges were embedded in solid granite and PMMA targets which were hit by a 700 J Pharos pulse.[2] The ruby gauges were placed 2 mm from the laser focus where the pressure was up to 80 kilobar and the shock risetime was less than 35 ns. The carbon gauges were placed 1 cm from the laser focus where the pressure was up to 6 kilobar and the shock risetime was 100 ns. In this manner the gauges' impulse response was measured. (Shocks in solids have a faster risetime (e.g. 100 ns at 10 mm) than shocks in water (300 ns at 12 mm).) (The cost of these experiments was leveraged by a DSWA contract to study shock coupling of above-ground explosions into underground structures.)

In addition to carbon and ruby gauges, piezoelectric film gauges were also tested in laser shock experiments in solids. The piezoelectric gauges cover a pressure range similar to the carbon gauges, but are more susceptible to electrical noise.

Laser plasma-generated electromagnetic pulse (EMP) noise dominated the electrical pressure gauge signals in solids unless several noise reduction techniques were used. Though less intense than in solids within vacuum and air environments, EMP noise is also a problem in water. Several EMP noise reduction techniques developed during

gauge tests in solids were later used effectively in these water experiments. These techniques are also described in detail in the next section.

To summarize results of pressure gauge tests in solids, carbon and ruby gauges were found to complement each other in sensitive pressure range. Ruby gauges are sensitive to higher pressures relevant to small radii, while carbon gauges are sensitive to lower pressures (which obtain over a larger volume in the water shock experiments). As described in the next section, the response time of carbon gauges is limited due to their finite size. In keeping with their smaller size, ruby gauges exhibited a faster time response. Finally, carbon gauges were found to require several measures to mitigate electrical noise while ruby gauges required a special coating or other shielding from stray light.

In addition, extensive diagnostics for imaging plasma light and density gradients associated with laser shocks have been developed within NRL Code 6795 for shock experiments in plastic, quartz, and air. These include schlieren imaging with a short-pulse laser for backlighting. This imaging technique provides high sensitivity to density gradients while fast time resolution and clear illumination are provided by an 300 mJ, 8 ns Nd:YAG laser pulse. A basic implementation of this diagnostic, seen in Fig. 1, was used in the water shock experiments.

Carbon Pressure Gauges

Carbon pressure gauges were fielded in these water experiments rather than the ruby gauges. Carbon gauges are sensitive to pressures from a few tens of bar to 50 kilobar, a range valid for a much larger volume in the water shocks than for the pressures measurable by ruby gauges. Further, ruby gauge tests in solids revealed a high sensitivity to stray light. A special coating for shielding the rubies from stray light in water, presently under development, will be necessary for water tests of these gauges. The different pressure regimes of gauges available for use in water shocks are shown in Fig. 2.

---

[2] J. Grun, C. Manka, R. Burris, T. Jones, T. Russell, G. Pangilinan, to be published.

The carbon pressure gauges used in these experiments were piezoresistive, meaning their resistance changes as a function of pressure. Gauges from Dynasen, Inc., Goleta, CA were used in our experiments. Both their standard 50 ohm gauges (type C300-50-EK) and their low-noise folded configuration gauges (type FC300-50-EK) were fielded. Gauge pressure is given by:[3]

$$p\ (kilobar) = 0.255\left(\frac{\delta R}{R}\right) + 0.00075\left(\frac{\delta R}{R}\right)^{2.2} + 0.0000021\left(\frac{\delta R}{R}\right)^{4},$$

where $\left(\frac{\delta R}{R}\right)$ is change in gauge resistance in percent. These gauges are calibrated with μs-timescale projectile-impulse tests in the range of tens of bar to approximately 50 kilobar.

Gauge resistance was measured using a Wheatstone impedance bridge in Quarter Bridge configuration.[4] The impedance bridge is shown in Fig. 3. A gated power supply drove 120 mA through the test gauge for approximately 100 μs. One leg of the impedance bridge consisted of a potentiometer for balancing the zero-pressure voltage. The impedance bridge was connected through 50 ohm impedance coaxial cable to the test gauge in the target chamber. Another cable connects a reference carbon gauge epoxied in material identical to the test piece. This reference gauge compensates for resistive changes in the test gauge due to temperature rise from the pulsed current. The gauges, connecting coaxial cables, and bridge circuit are all impedance matched at 50 ohms, minimizing signal reflections and related noise. The bridge circuit and power supply are enclosed in a metal case to provide shielding from electrical noise, and the bridge circuit, reference gauge, and digitizer are located in an electromagnetically shielded room.

Successful EMP noise reduction techniques included the use of: rigid coaxial signal lines (utilizing high-conductivity outer conductors), high-inductance ferrite filters (these suppress ground-loop currents caused by the signal cable coupling to stray

[3] From calibration curve in Dynasen, Inc. "Shock Pressure Sensors and Impact Facility" catalog, dated March 17, 1994.

[4] The Wheatstone bridge circuit design was provided by M. Voss at Boeing Defense and Space Group, Seattle, WA.

capacitances in surrounding structures), and spatial isolation from the plasma shock source which provides a time delay for shock arrival sufficient for EMP noise to decay. Special signal clipping circuitry was also built to minimize amplifier saturation during the brief initial EMP pulse. Good signal to noise ratio was obtained using these techniques at distances as close as 8 mm.

Response time of the carbon gauges was limited by the shock transit time across the gauge, so smaller gauges provided faster response times. The carbon element was 13 μm thick, yielding a transit time of 4 ns for planar shocks incident perfectly normal to the plane of the carbon. Shock sphericity spreads the arrival time across the element since the curved shock front does not all pass through the gauge at a single time. At 5 mm and normal incidence, the shock front arrival is spread by up to 200 ns. Care must be taken to ensure that the gauges are normal to shock incidence to keep shock transit time to a minimum. The smallest carbon gauges available were 0.050 x 0.050 inches in the standard configuration, and 0.050 x 0.100 inches in the folded gauge configuration. Due to their much reduced susceptibility to EMP noise, the folded gauges were used for data presented here.

Carbon piezoresistive gauges yielded good signal to noise ratio in these water experiments at distances as close as 1 cm. At small distances (< 6 mm), the carbon gauges did not provide reliable measurements. Their signal to noise ratios were low and/or they were destroyed during the experiment. Ruby gauges should be able to operate at these distances and pressures.

Optical Diagnostics

Laser focusing and plasma breakdown were monitored by imaging visible light using a CCD camera. The camera image was digitized with a frame-grabber and analyzed on a PC. Different filters were used to selectively image either scattered light at the doubled Pharos laser frequency, or all other light as in the image in Fig. 4.

The above-mentioned schlieren imaging with pulsed laser backlighting was used to image both shock and bubble formation (see Figures 7 and 8). Shock propagation speed measured in schlieren images was used to infer shock pressures at small radii. These pressures supplement measurements by carbon piezoresistive at large shock radii (see Fig. 2). Shock and bubble images also provided a measure of shock reproducibility, as well as an independent pressure measurement. These results are discussed in the next section.

Laser Shock Generation

Our experiments demonstrated successful focusing in water at $f/\# = 1.6$ for energies up to 150 J. No pinching or other beam instability was observed in visible images before the beam reached focus.

Several shots were taken at high laser energy with the laser focused at a spot in the water (no solid target). Imaging of the 527 nm scattered light revealed that the laser beam was not completely stopped in the breakdown plasma at the beam focus, but continued on at high intensity for several mm. The beam appeared to produce an elongated plasma along the beam axis near the focus. Schlieren imaging revealed that an elongated shock was also produced (see Fig. 4), potentially creating an elongated bubble as well. Because of this tendency for distributed laser energy deposition near focus, solid targets are required at the laser focus to localize energy deposition. Laser shots with solid targets showed no evidence of beam propagation beyond the target, indicating that the laser energy was successfully deposited on the film surface. After these initial shots the laser was therefore focused onto solid targets in all subsequent shots. Shock and bubble dynamics results discussed below all pertain to laser shock generation from solid targets.

Some broadband light was observed emanating from the focal volume just in front of the focus, extending approximately 4 mm along the beam axis from focus. This light

was interpreted as evidence of atomic excitation or possibly low-level ionization of the water.

Two types of solid, thin film targets were used in these experiments: 1) a 2 μm thick Kimfol (plastic polyamid) foil with a 13 nm Aluminum layer on one side, and 2) a 25 μm thick Upilex (plastic) foil. The 2 μm Kimfol target was used first because it was the thinnest available opaque material. This foil was cut into long, 1 cm wide strips and suspended in the water with a weight at one end. For all shots with 2 μm foil, the target was located approximately 4 mm in front of the beam focus to avoid beam propagation through the region that might be ionized. At this target location, the beam spot size was approximately 2.5 mm. As discussed in the Shock Dynamics section, shock shape at small radii was influenced by the target shape. In some shots, planar shocks were observed launching from the foil strip during the laser pulse. This phenomenon was not observed with the Upilex targets, and was likely caused by the elongated geometry of the Kimfol. These planar shocks, along with the difficulty of reproducibly locating the suspended Kimfol and its tendency to drift in position, motivated a change to Upilex targets.

The 25 μm thick Upilex targets were cut into small strips approximately 2 mm x 7 mm, and epoxied into a groove in the end of a 2 mm diameter wooden dowel. The wooden dowel was then placed in an optical mount resting on the bottom of the water chamber. The Upilex was rigid enough to stand up vertically from the support dowel. The smaller size of the Upilex targets (resulting in shocks that are more spherical), their positional stability, and the lack of planar shock generation made the Upilex targets superior to the Kimfol. Several shots were also taken with the Upilex targets located exactly at the beam focus, with no detectable difference in shock propagation at 6 μs or pressure measured by carbon gauges at 6 mm. Fears of beam absorption or reflection in the emitting water volume just in front of focus were therefore unfounded.

Shock dynamics

Using both types of solid targets, laser-plasma generated shocks were observed over a broad range of incident laser energies (from a fraction of a Joule to approx. 150 Joules). These shocks had reproducible propagation speeds and shapes. Three shots were taken with the same laser energy and target. Shock propagation distances at 15 μs (which determine the average shock speeds from t = 0) were within 10% of each other for a spread in laser pulse energy of approximately 10%. At small radii, the shocks formed an ellipsoid centered at the beam spot and elongated along the plane of the foil. The shocks became spherical at radii greater than the approximate dimension of the foil (approximately 8 mm for the 2 mm x 7 mm Upilex targets).

The shock pressure at small radii (r < 5 mm) and early times (t < 3 μs) was inferred from shock propagation distances. This was the only available technique for determining pressure at these radii at the time, as coated ruby gauges were not ready. At t = 880 ns after the Pharos beam pulse the shock radius was 2.9 mm, yielding an average shock expansion velocity from time t = 0, $v_{avg} \equiv r/t = 3.3$ mm/μs. Shock pressure can be related to shock speed using the empirical formula:[5]

$$p = \left(\frac{1}{2.1}\right)\rho_o v(v - v_o),$$

where ρ_o is the unperturbed water density, v_o is the speed of sound in water, and v is the shock speed. Substituting v_{avg} for v yields a pressure $\bar{p} \equiv p(v = v_{avg}) = 29$ kbar. This inferred shock pressure is valid at the radius (inside 3 mm) where $v = v_{avg}$. The initial pressure at the target is higher. Fig. 5 shows a plot of shock radius as a function of time as well as v_{avg}.

The shock pressure was measured directly with a carbon gauge at a 13 mm distance from the laser plasma to be approximately 200 bar and is shown in Fig. 6. (The shock pressure signal is observed starting at 8 μs, with a laser plasma-generated noise

[5] Yu S. Yakovlev, Explosion Hydrodynamics (in Russian), Sudpromgis, Leningrad (1961).

precursor which dies out by 5 μs, as described in the Carbon Gauge section above.) At 5 mm, v_{avg} was within 20% of the sound speed. At distances greater than 10 mm shock propagation speed was within measurement error of sound speed.

Bubble formation

At late times (t > 100 μs), the initial laser plasma volume created by the laser was seen to expand into a spherical bubble (see Fig. 7). For the maximum laser energies (approximately 150 J), the bubble expansion time was on the order of 1 ms and the maximum radius was approximately 15 mm. Both maximum bubble radius and bubble expansion velocity were observed to increase with laser energy. The bubble was observed to collapse again to a minimum radius at approximately 3 ms. A second bubble expansion was observed subsequently, consistent with bubble oscillations observed in previous experiments[6].

At the highest laser intensities ($I > 10^{10}$ W/cm^2), some beam energy was deposited in the focal volume in front of the beam focus as evidenced by shocks generated at the boundaries of this conical volume (see Fig. 8). These were interpreted as being caused by rapid heating and expansion of the water in the focal volume during the 5 ns laser pulse. These shocks may be mitigated by focusing at a smaller f/# (steeper focusing angle). In schlieren images the shock generated by the focal cone can be seen to propagate at the sound speed in water even at early times (t < 1 μs). These slow early shock speeds indicate much lower pressures (v_{avg} within 10% of sound speed within in the first 3mm of propagation, corresponding to $\overline{p} < 1$ kbar) compared to the shock generated by the laser plasma at the target. In addition, as seen at late times, this shock does not form a large bubble as does the laser plasma at the target (see Fig. 7).

[6] P. Testud-Giovanneschi et al., J. Appl. Phys. **67**, 3560 (1990).

The shocks launched from the focal volume were the only observed qualitative difference from previous laser shock generation experiments performed with laser pulse energies on the order of 1 Joule.[7,8,9]

2) Chamber Design

Following is a list of design elements for the final chamber design determined by these experiments:

1. The focusing volume for the Pharos beam can be in either vacuum or water for shock and bubble dynamics experiments.
2. For laser focusing in vacuum, a conical evacuated focusing chamber will be placed at the chamber side within the water chamber. A foil laser target will cover the tip of the focusing chamber, serving as the point of shock generation
3. For laser focusing in water, focusing optics will incorporate large focusing angles and f/# ~ 1 or less to minimize the water volume with the highest intensity beam path. The final focusing lens will either serve as the chamber window or be adjacent to it in order to minimize beam intensity on the window while maximizing distance from the focus to the chamber wall.
4. The chamber will be metal with dimensions approximately 1 m x 1 m x 1 m. Flat sides will provide for easy mounting of windows and ports. For a maximum laser energy of 500 J, shock pressures of 30 kbar will be produced in a volume approximately 1 cm in diameter, and shock pressures of 200 bar in a volume approximately 4 cm in diameter.
5. The chamber will incorporate at least four large optical quality windows. Two 20 cm diameter windows will provide Pharos beam access on opposite sides of the chamber. The remaining two large (also 20 cm diameter) windows will provide access for both imaging and backlighting, so that bubbles on the order of 20 cm diameter can be

[7] A. Phillip and W. Lauterborn, J. Fluid Mech. **361**, 75 (1998).
[8] P. Testud-Giovanneschi, Ibid.

imaged. Several small ports will provide other diagnostic access including: electrical and fiber optic feed-throughs for at least 10 pressure gauges of either electrical or optical type, sand diagnostics, and controls for a motorized laser target.

6. A plate with ¼ - 20 tapped boltholes in a regular 1 or 2-inch pattern will be installed on the bottom of the chamber for mounting equipment.
7. A motorized stage for laser targets used in experiments in pure water will be mounted from the top of the chamber. These laser targets will be "lollipop-shaped" targets with the target area made of thin foil one or two mm in diameter, supported by as small a support stalk as possible to minimize interaction with shocks and bubbles.
8. Experiments will be conducted with an air volume over the water to allow for expansion of the water volume during bubble formation, thus stabilizing the ambient water pressure for experiments.
9. The vacuum chamber will be sealed to allow drawing a partial vacuum (~100 Torr) to increase bubble size. The chamber should also allow pressurization (~50 psig) for preparation of sand/water mixtures. Air pumping and pressurization ports with splashguards will be installed at the top of the chamber.
10. The chamber water will be continuously circulated through a filtration and deionizing system to maintain water quality sufficient to operate immersed electrical gauges. Temperature regulation capable of heating the chamber to approximately 70 C for sand preparation will be incorporated into the water treatment system.
11. The chamber will incorporate hardware (to be designed and built by NRL Code 7400) providing support for a compacted sand layer approximately 20 to 50 cm thick

The detailed design of the final experimental chamber is presently in progress, and materials procurement has begun.

[9] W. Lauterborn, Appl. Sci. Res. **38**, 165 (1982).

Summary of Progress

1. A temporary water chamber with one incident beam of the Pharos laser was set up and used for preliminary water shock initiation experiments. These experiments confirmed the feasibility of high energy laser-generated shock and bubble generation in water with the Pharos laser.
2. Laser generated water shocks were successfully generated with up to 150 J of 527 nm laser energy. The incident beam was successfully focused in water onto thin (few micron thickness) plastic targets, with shocks centered at the area of laser incidence.
3. Shock pressure at maximum laser energy was inferred from shock speed, and was greater than 30 kbar within radii up to ~ 2 mm.
4. Shock reproducibility was good. For fixed incident laser energy, shock velocity, sphericity, and peak pressure at 12 mm were identical to within the laser reproducibility error (~ 15%).
5. Shocks were observed to be spherical at distances greater than twice the target dimension (targets as small as 2 mm were used in our preliminary experiments).
6. Spherical bubbles were observed to form after the initial shock, also centered at the area of laser incidence on the target. The maximum bubble radius was approximately 3 cm with an oscillation time of approximately 3 ms. There is a capability to produce larger bubbles, either by pulling a partial vacuum on the water chamber or by coupling more laser energy with two beams. Larger bubbles make imaging easier, and reduce the scaling factor to full-scale underwater explosions.
7. Pressure measurements were made with carbon piezoresistive gauges.
8. The basic design for the permanent experimental chamber has been determined based on results 1–7 above from these experiments. Detailed design and materials procurement for the permanent chamber is in progress.

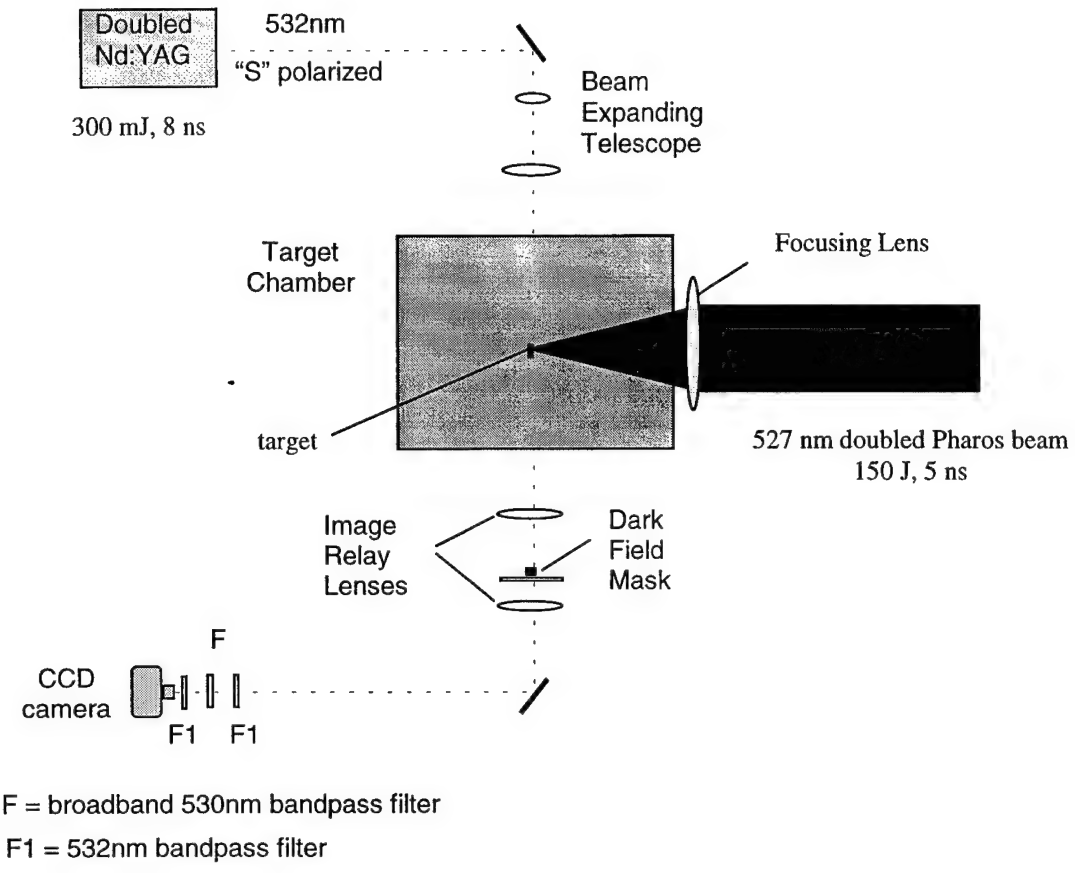

Figure 1. A schematic of the experimental setup is shown. The schlieren imaging system with Nd:YAG laser backlighting is shown in the configuration used to observe shock and bubble formation. For schlieren imaging, the above bandpass filters were used to exclude all light except that from the Nd:YAG backlighting laser. For initial experiments aimed at testing laser focusing, only the CCD camera with imaging lenses and filters was used. For these initial images, filters were alternately chosen either to view scattered 527 nm Pharos light (bandpass filters) or to block 527 nm and image the broadband light (notch filters), which was presumably from the laser plasma.

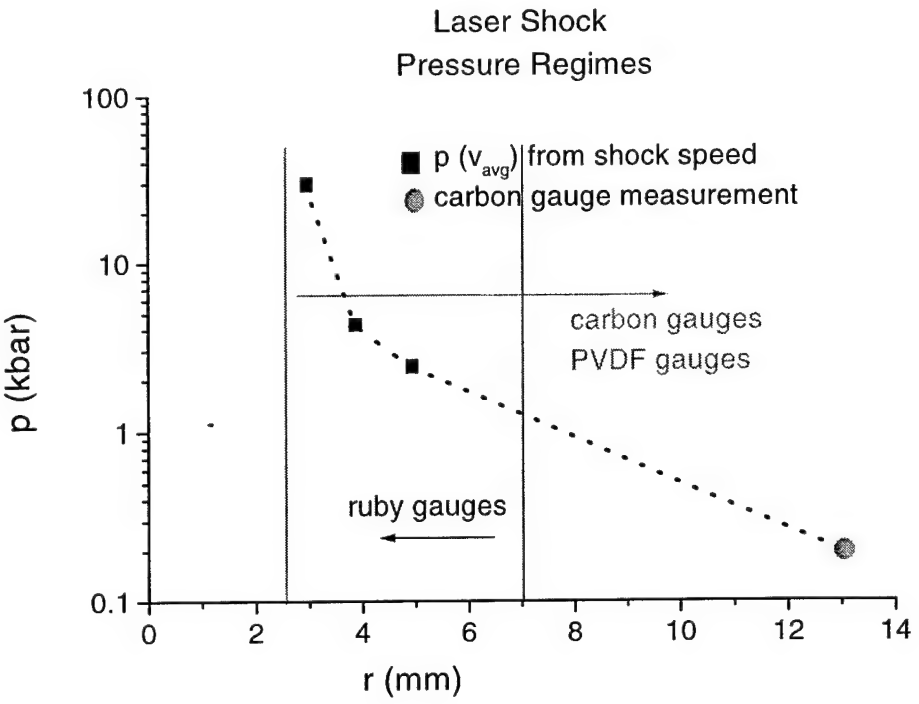

Figure 2. A plot of shock pressures is shown as a function of radius from the laser plasma. Pressures inside 5 mm were inferred from shock speeds as measured in schlieren images, and the pressure measurement at 13 mm was measured by a carbon piezoresistive gauge. Effective regimes of gauge sensitivities are overlaid on the pressure plot, indicating at what distances each type of gauge can be used. Shocks were observed to become spherical at roughly twice the dimension of the solid target (~ 8 mm in shots with the Upilex targets).

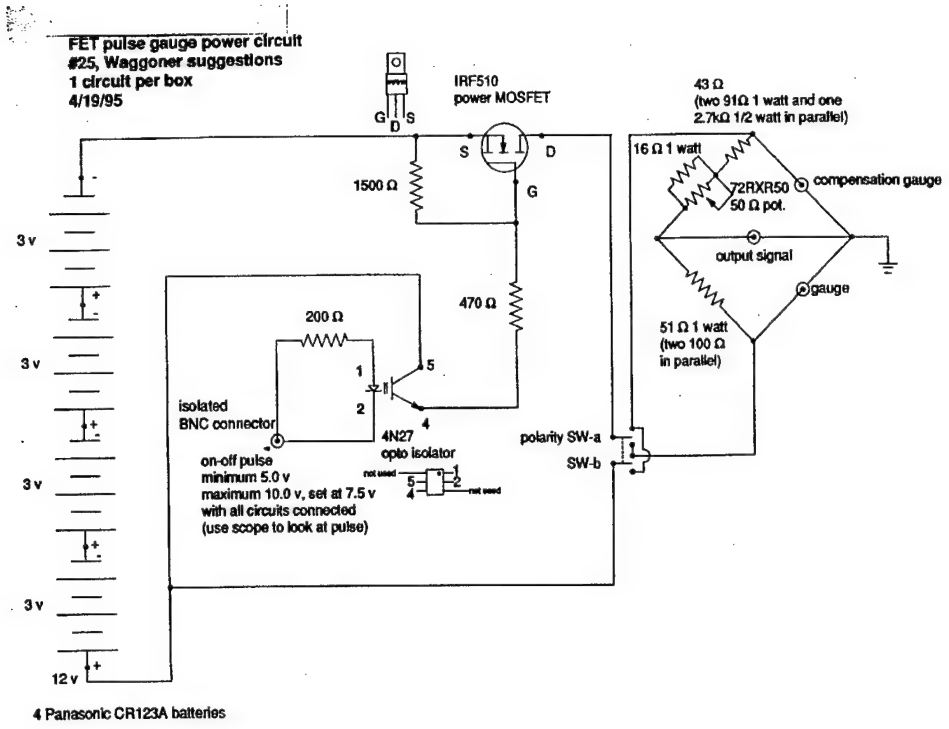

Figure 3. The impedance bridge used to measure carbon gauge resistance is shown. A gated power supply drives 120 mA through the test gauge for approximately 100 μs. One leg of the impedance bridge consists of a potentiometer for balancing the zero-pressure voltage. The impedance bridge is connected through 50 ohm impedance coaxial cable to the test gauge in the target chamber. Another cable connects a reference carbon gauge epoxied in material identical to the test piece. This reference gauge compensates for resistive changes in the test gauge due to temperature rise from the pulsed current.

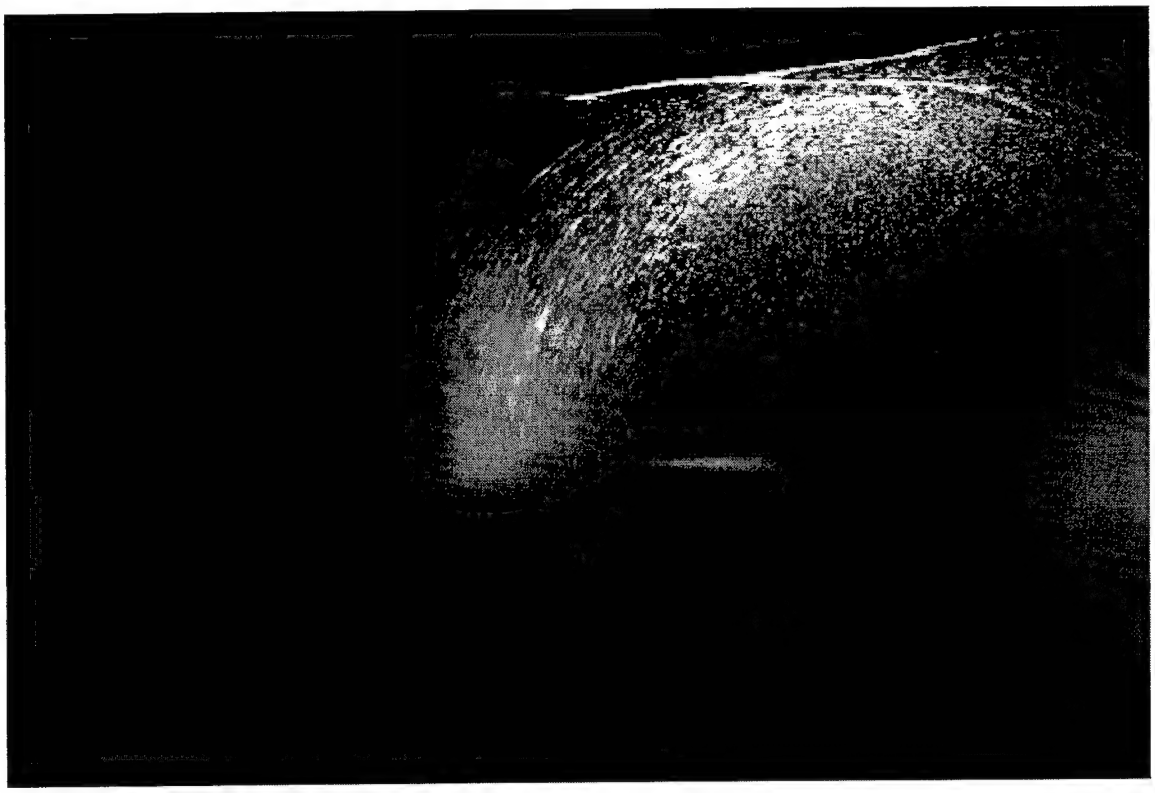

Figure 4. The laser beam is horizontal and incident from the right in the frame. The medium is water and there is no solid target for this shot. The field of view is approximately 3 cm height by 4 cm width. The elongated bright spot near the middle of the frame is plasma light. With greater optical density filters, this can be seen as a series of elongated light sources. At the top of the field of view, the envelope of the shock fronts created along the laser plasma can be seen as a bright horizontal line. The corresponding shock envelope image underneath the laser plasma is out of the field of view.

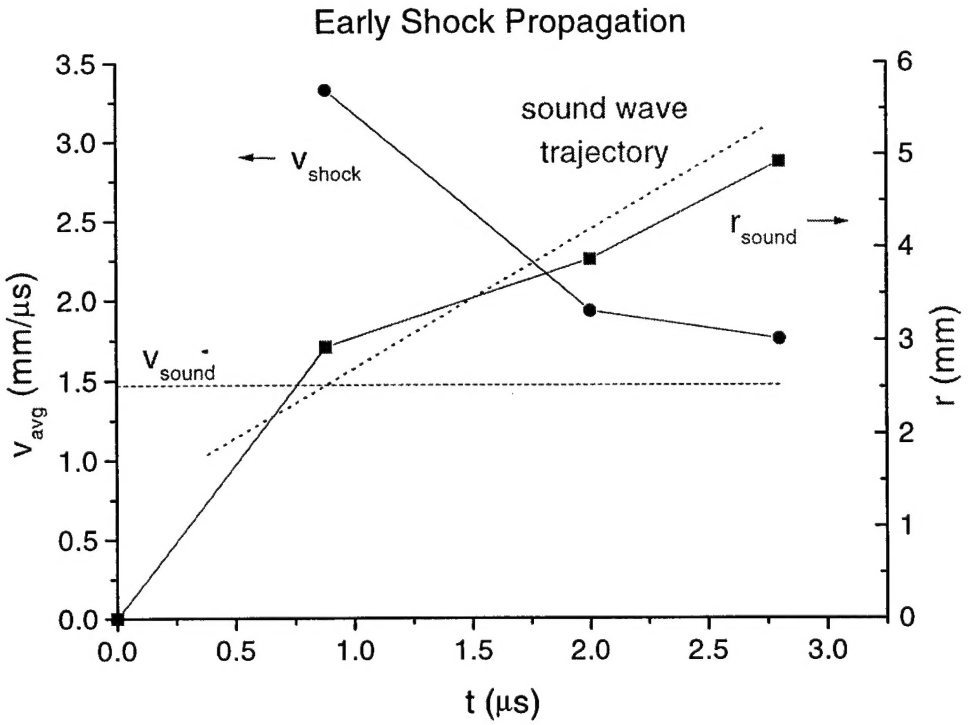

Figure 5. Early shock propagation ($t < 3$ μs) was measured from schlieren images in a set of three shots. Shock radius is shown in mm (scale at right), and *average* shock velocity from $t = 0$ as a function of time (r/t) is shown in mm/μs (scale at left).

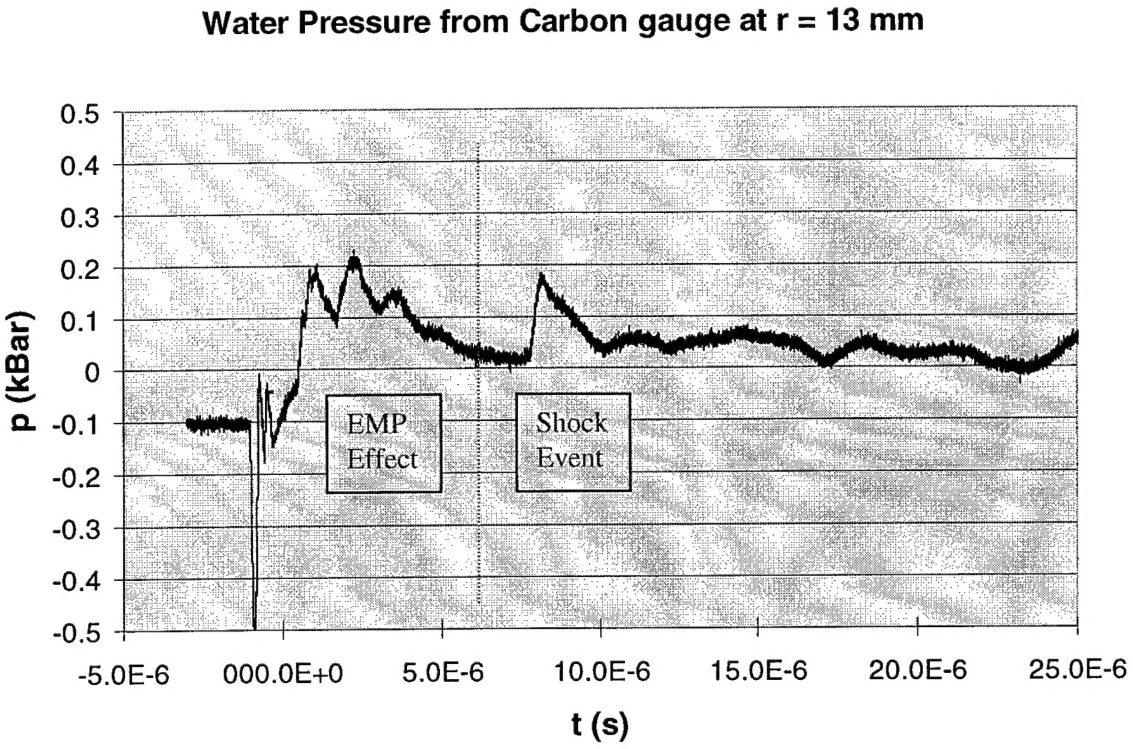

Figure 6. A pressure trace from a carbon piezoresistive gauge is shown. The gauge was located 12 mm from the laser plasma. (The mounting block for the gauge can be seen in the upper left of Fig. 8.) The gauge biasing circuit is turned on at –1 μs and the laser fires at t= 0. The laser energy for this shot is approximately 120 J. The peaks in the signal before 5 μs are noise from EMP caused by the laser plasma. The shock pressure signal is seen at 8 μs with an amplitude of just under 200 bar in this shot.

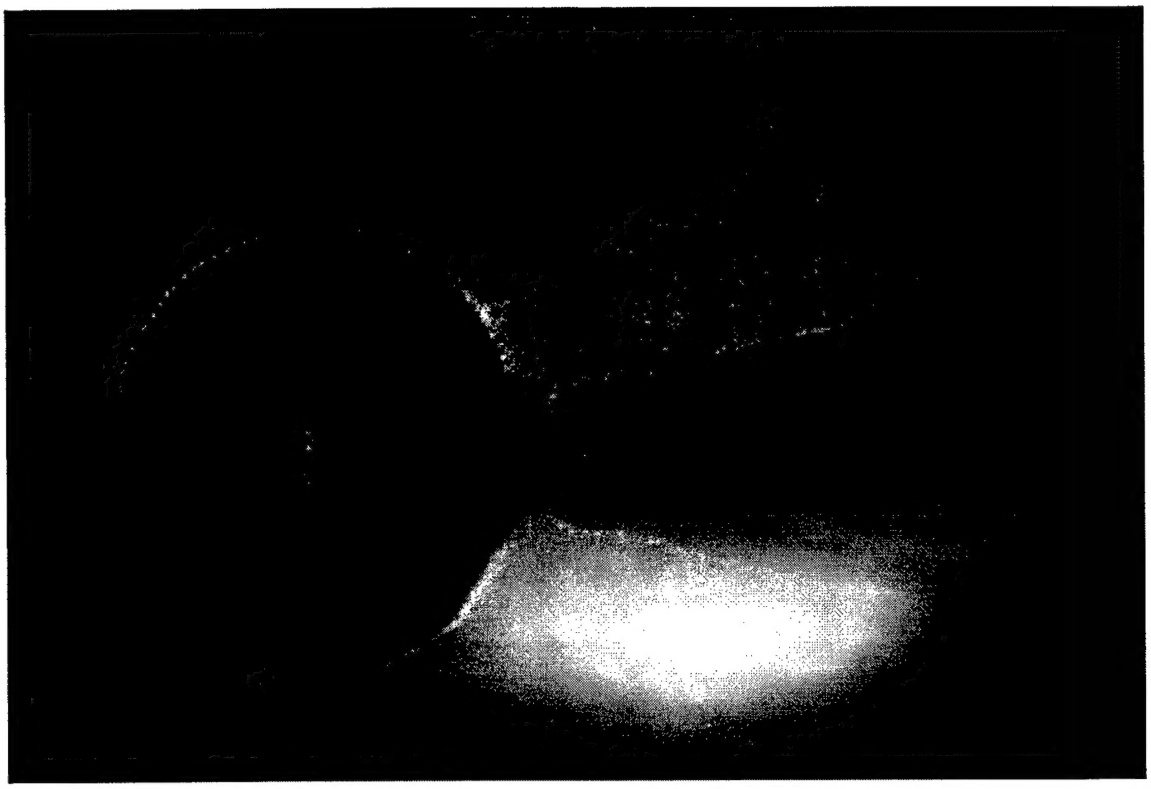

Figure 7. A schlieren image shows bubble formation at 200 μs after the laser pulse during bubble expansion. The bubble diameter at this time is approximately 2 cm, eventually reaching a maximum of 3 cm at 1500 μs. The laser is incident from the right with and energy of approximately 150 J. The opaque conical laser focal volume on the right is interpreted as caused by refraction through water heated during the laser pulse to higher temperature than the surrounding water.

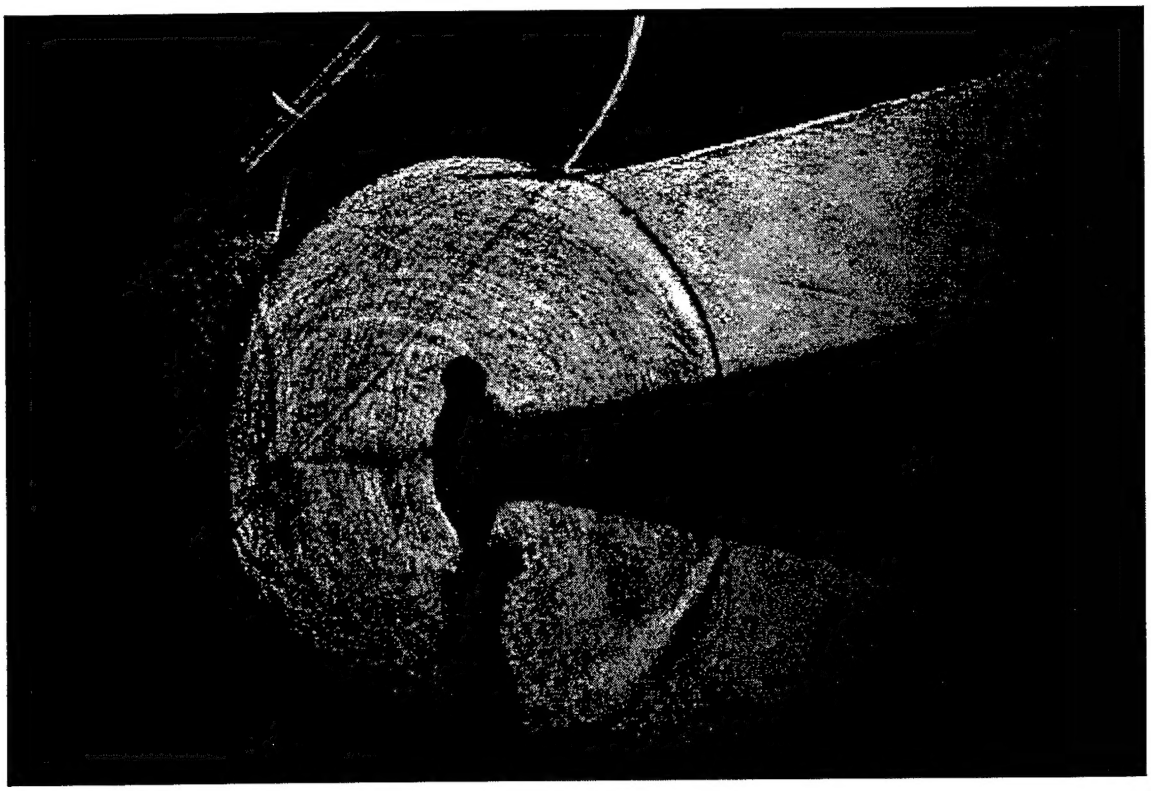

Figure 8. A schlieren image shows a spherical shock generated by the laser plasma at the target at 6 μs after the laser pulse. The laser energy is approximately 150 J. A conical shock can also be seen at the right side of the frame caused by rapid heating and expansion of water in the focal volume (dark conical volume).